Molecular Imaging of Matrix Metalloproteinase Activation to Predict Murine Aneurysm Expansion In Vivo

Mahmoud Razavian*[1,2], Jiasheng Zhang*[1,2], Lei Nie[1,2], Sina Tavakoli[1,2], Niema Razavian[1,2], Lawrence W. Dobrucki[1], Albert J. Sinusas[1], D. Scott Edwards[3], Michael Azure[3], and Mehran M. Sadeghi[1,2]

[1]Cardiovascular Molecular Imaging Laboratory, Section of Cardiovascular Medicine, Yale University School of Medicine, New Haven, Connecticut; [2]Veterans Affairs Connecticut Healthcare System, West Haven, Connecticut; and [3]Lantheus Medical Imaging, North Billerica, Massachusetts

Rupture and dissection are major causes of morbidity and mortality in arterial aneurysm and occur more frequently in rapidly expanding aneurysms. Current imaging modalities provide little information on aneurysm beyond size. Matrix metalloproteinase (MMP) activation plays a key role in the pathogenesis of aneurysm. We investigated whether imaging MMP activation in aneurysm helps predict its propensity to expansion. **Methods:** We used a model of carotid aneurysm in apolipoprotein E–deficient (apoE$^{-/-}$) mice. Radiotracers with specificity for activated MMPs were used to detect and quantify MMP activation by micro-SPECT/CT in vivo. Tracer uptake was confirmed by autoradiography and γ-well counting, and specificity was demonstrated using an excess of unlabeled precursor and a specific MMP inhibitor. **Results:** We demonstrated that several MMPs are expressed with distinct temporal patterns in aneurysm. Significant focal uptake was observed in aneurysmal carotid arteries, peaking at 4 wk after aneurysm induction. In a group of animals imaged serially at 2 and 4 wk after aneurysm induction, MMP tracer uptake at 2 wk correlated well with the vessel area assessed by histology at 4 wk. **Conclusion:** Molecular imaging of MMP activation is a useful experimental, and potentially clinical, tool to noninvasively predict the propensity of an aneurysm to expansion in vivo.

Key Words: nuclear imaging; matrix metalloproteinases; aneurysm

J Nucl Med 2010; 51:1107–1115
DOI: 10.2967/jnumed.110.075259

Aneurysm, focal dilation of large arteries, is a prevalent disease of various vascular beds, including the abdominal and thoracic aorta, iliac arteries, and popliteal arteries. The pathogenesis of aneurysm commonly involves inflammation, protease activation, extracellular matrix remodeling, and vascular smooth muscle cell (VSMC) dysfunction and apoptosis, which ultimately lead to weakening of the vessel wall and arterial expansion under the influence of mechanical forces (*1,2*). Rupture, dissection, and distal embolization are frequent and highly morbid complications of aneurysm. Although size is the best predictor of the risk of complications, rapid expansion also increases the propensity of an aneurysm to rupture or dissection. Current practice guidelines recommend surgical treatment for large aneurysms and monitoring by serial imaging for smaller aneurysms (*3*). However, many complications occur in smaller aneurysms that do not meet the criteria for surgical repair (*4,5*). Prospective identification of such smaller aneurysms that are at high risk for complications can tilt the risk–benefit balance toward early treatment and reduce aneurysm morbidity and mortality.

Matrix metalloproteinases (MMPs), a multigene family of endopeptidases that selectively digest individual components of the extracellular matrix, play a key role in the pathogenesis of aneurysm and its complications, rupture, and dissection (*6–9*). MMPs are biosynthesized as inactive secreted or transmembrane proenzymes, which are activated through enzymatic cleavage of the propeptide domain. This exposes a catalytic domain that may be targeted for imaging using specific probes (*10*). Imaging targeted at molecular markers of disease activity provides a unique opportunity to elicit information on the pathogenic process in vivo. The central role of MMP-mediated matrix remodeling in arterial aneurysm raises the possibility that MMP-targeted imaging may detect the propensity of an aneurysm to expansion in vivo. Here, we use a family of radiotracers with specificity for the activated MMP catalytic domain (*11*) to image MMP activation in murine carotid aneurysm in vivo. We show that MMP-targeted imaging reflects MMP activity detected by zymography in the vessel wall and demonstrate that molecular imaging of MMP activation in vivo provides unique information on the molecular properties of an aneurysm that are related to expansion.

Received Jan. 19, 2010; revision accepted Mar. 17, 2010.
For correspondence or reprints contact: Mehran M. Sadeghi, Veterans Affairs Connecticut Healthcare System, 950 Campbell Ave., West Haven, CT 06516.
E-mail: Mehran.sadeghi@yale.edu
*Contributed equally to this work.

MATERIALS AND METHODS

Reagents

Reagents were from Sigma, unless otherwise specified. RP782, an ^{111}In-labeled tracer with specificity for activated MMPs, and the precursor for its ^{99}Tc-labeled homolog, RP805 (*11*), were provided by Lantheus Medical Imaging. RP805 radiolabeling was performed according to the manufacturer's instructions. The structure, binding characteristics, and biodistribution of MMP tracers in mice were previously reported (*11–13*).

Animal Model

Arterial aneurysm was induced by exposing the left common carotid artery of apolipoprotein E–deficient (apoE$^{-/-}$) mice to calcium chloride as described previously, with modifications (*14*). This model reliably leads to the development of a large aneurysm in many animals. Briefly, 4- to 6-wk-old female apoE$^{-/-}$ mice (n = 96; Jackson Laboratory) were fed high-cholesterol chow (1.25% cholesterol; Harlan Teklad) ad libitum. After 1 wk, the carotid arteries were exposed by blunt-end dissection under anesthesia (ketamine, 100 mg/kg; xylazine, 10 mg/kg, intraperitoneally). The left common carotid artery just below the carotid bifurcation was adventitially exposed to a 10% solution of $CaCl_2$ for 20 min. The opposite carotid artery was exposed to normal saline and served as a control for imaging studies. Ibuprofen (0.11 mg/kg/d, by mouth) was used for postoperative analgesia. Experiments were performed according to regulations of Yale University's Animal Care and Use Committee.

Histology, Morphometry, and Immunofluorescent Staining

Animals were anesthetized at 2, 4, or 8 wk after surgery. After perfusion with normal saline, the carotid arteries were harvested, embedded in optimal-cutting-temperature compound, snap-frozen, and stored at −80°C until further use. Elastic van Gieson staining and immunostaining were performed according to standard protocols on 5-μm-thick cryostat sections. For morphometric analysis, microscopic measurements were performed on cryostat sections with ImageJ software (National Institutes of Health), as previously described (*15*). The area within the external elastic lamina (total vessel area) was calculated by averaging measurements from 10 sections at 200-μm intervals from 200 to 2,000 μm below the carotid bifurcation. For immunostaining, primary antibodies included antimouse MMP-2, -7, -9, and -12 (Chemicon); anti–smooth-muscle α-actin (Sigma); anti-CD31 (BD Pharmingen); and F4/80 (Invitrogen). Isotype-matched antibodies were used as controls. Nuclei were detected with 4′,6-diamidino-2-phenylindole (DAPI). The slides were photographed with a fluorescent microscope equipped with a digital camera (Zeiss).

Zymography

In situ gelatinase zymography was performed using an EnzCheck Gelatinase Assay Kit (Molecular Probes) according to the manufacturer's instructions, with a minor modification. Briefly, 5-μm-thick frozen sections were incubated with buffer (50 mM Tris-HCl, 150 mM NaCl, 5 mM $CaCl_2$, and 0.2 mM sodium azide, pH 7.6) in the presence or absence of MMP inhibitor (10 mM 1,10-phenanthroline) for 15 min at 37°C. Next, DQ gelatin solution (0.1 mg/mL in phosphate-buffered saline; Molecular Probes) and DAPI were added, and the sections were incubated at 37°C for 60 min. The slides were photographed using a fluorescent microscope equipped with a digital camera.

MMP activity of protein extracts was assessed using a Fluorimetric SensoLyte 520 Generic MMP Assay Kit (AnaSpec) according to the manufacturer's instructions. This kit detects the activity of several MMPs, including MMP-1 to -14. Total protein was extracted from the carotid arteries using a lysis buffer (50 mM Tris-HCl, pH 7.4; 300 mM NaCl; 1% Triton X-100; and ethylenediaminetetraacetic acid–free protease inhibitor cocktail [Roche]). MMP activity was quantified by measuring fluorescence intensity after 1 h at 37°C and is presented as background-corrected fluorescence intensity per microgram of protein. The performance of the kit, which was used within its linear range, was validated in preliminary studies using recombinant active MMP-9 (not shown).

Quantitative Reverse-Transcription Polymerase Chain Reaction (PCR)

Total RNA was isolated from the carotid arteries using an Absolutely RNA Nanoprep Kit (Stratagene) and reverse-transcribed using a QuanTitect Reverse Transcription Kit (Qiagen). Quantitative PCR was performed on this cDNA in triplicate using Taqman primers (Applied Biosystems) and a 7500 Real-Time PCR System (Applied Biosystem) following the manufacturer's instructions. The specificity of PCR amplifications was confirmed by running PCR products on agarose gels. The results were normalized to glyceraldehyde 3-phosphate dehydrogenase. The following primer sets were used: MMP-2 (Mm00439506_m1), MMP-3 (Mm00440295_m1), MMP-9 (Mm00442991_m1), MMP-12 (Mm00500554_m1), MMP-13 (Mm01168713_m1), and glyceraldehyde 3-phosphate dehydrogenase (Mm99999915_g1).

Imaging

Thirty-seven (±1.12) MBq of RP782 (^{111}In-labeled) (*11*) were administered to groups of animals at 2, 4, and 8 wk after $CaCl_2$ exposure through a right jugular intravenous catheter. Animals were imaged after 2 h on a high-resolution small-animal imaging system (X-SPECT; Gamma Medica-Ideas) with 1-mm medium-energy collimators (*12*). Anesthetized mice (under isoflurane) were placed in a fixed position on the animal bed. Three point sources of known activities (37–185 kBq) were placed in the field of view but outside the body to quantify uptake and verify the accuracy of image fusion. The following acquisition parameters were used for micro-SPECT: 360°, 128 projections, and 30 s/projection (~80 min of image acquisition), with 174- and 242-keV photopeaks ± 10% window (for ^{111}In). After the completion of micro-SPECT, animals were injected with a continuous infusion of iodinated CT contrast (iohexol, 100 μL/min) over 2 min, and CT was performed (energy, 75 kVp/280 μA; matrix, 512 × 512) to identify anatomic structures. The imaging protocol lasted approximately 1.5 h, after which (3.5 h after tracer administration) different tissues were harvested for autoradiography or γ-well counting. To establish imaging specificity, a 50-fold excess of unlabeled precursor was administered to a group of animals 15 min before RP782 administration. For longitudinal imaging experiments, a group of animals (n = 11) underwent repeated imaging with RP805 (^{99}Tc-labeled) (*11*) at 2 and 4 wk. 1,3-Bis-[7-(3-amino-2,4,6-triiodophenyl)-heptanoyl]-2-oleoyl glycerol (HODG) (200 μL) (Fenestra-VC; ART Advanced Research Technologies) was used as the CT contrast agent in this group. The imaging protocol was similar to the one used for RP782, with the exception of the low-energy pinhole collimators and 140-keV photopeak ± 10% window used for ^{99m}Tc imaging. RP805 images were in

general of better visual quality than those obtained using ^{111}In-labeled RP782, although we did not detect any quantitative difference in carotid uptake between the 2 tracers. For quantitative analysis of tracer uptake, cylindric regions of interest were drawn at the level of carotid artery bifurcation ($2 \times 2 \times 2$ mm). A region of interest immediately posterior to both carotids was used to calculate the background activity. Data were expressed as background-corrected counts per voxel (cpv)/MBq injected.

Autoradiography and γ-Well Counting

A group of harvested carotid arteries was exposed to high-sensitivity, X-radiographic X-OMAT Kodak Scientific Imaging Film (Eastman Kodak) for various times to optimize detection. A set of standards with known activity deposited on Whatman paper (Whatman/GE Healthcare) was used to ascertain linearity of the signal. Other carotids were used for quantifying tracer uptake by γ-well counting. Given their small size, the carotids could not be accurately weighed. Therefore, 3-mm sections of the artery proximal to carotid bifurcation were used for uptake measurements. Data were background- and decay-corrected and expressed as counts per minute (cpm)/MBq injected.

MMP Specificity Assay

Five-micrometer-thick sections of the left carotid artery at 4 wk after surgery were incubated with 1,10-phenanthroline, a broad-spectrum MMP inhibitor (10 mM; Invitrogen), or control buffer for 15 min at 37°C. Next, RP782 (37.0 kBq) was added to tissues for 30 min at 37°C. After 3 washes, the samples were transferred to a tube for γ-counting.

Statistical Analysis

Statistical analysis was performed using GraphPad Prism (GraphPad Software). Data are presented as mean ± SE. Differences between 2 groups were tested using a 2-tailed unpaired Student *t* test, paired *t* test, or paired *t* test after logarithmic transformation for nonparametric data (ratio *t* test), as indicated. Multiple groups are compared using 1-way ANOVA (for parametric data) or the Kruskal–Wallis test (for nonparametric data), followed by, respectively, Tukey or Dunn post hoc analysis. The nonparametric Spearman or parametric Pearson correlation was used to test the association between 2 variables, as indicated. Significance was set at the 0.05 level.

RESULTS

Carotid Aneurysm in ApoE$^{-/-}$ Mouse

Arterial aneurysm was induced by exposing the left common carotid arteries of apoE$^{-/-}$ mice on a high-cholesterol diet to $CaCl_2$, leading to progressive expansion of the artery over a period of 8 wk (Fig. 1A). Elastic van Gieson staining demonstrated the straightening of elastic laminae and areas of discontinuity at 2 wk that progressed to almost complete dissolution of the membranes by 8 wk. The cross-sectional area of the left carotid arteries was significantly higher than that of the saline-treated, control right carotid arteries at 2 (0.26 ± 0.05 vs. 0.10 ± 0.01 mm^2, $n = 9$, $P = 0.01$), 4 (0.30 ± 0.03 vs. 0.09 ± 0.01 mm^2, $n = 13$, $P < 0.001$), and 8 wk (0.55 ± 0.11 vs. 0.12 ± 0.01 mm^2, $n = 10$, $P < 0.01$) after surgery (Fig. 1B).

CD31 immunofluorescent staining confirmed the presence of a relatively preserved endothelium surrounding the lumen in aneurysmal (left) carotid arteries at 4 wk after surgery (Supplemental Fig. 1; supplemental materials are available online only at http://jnm.snmjournals.org). Several neovessels were detectable in the adventitia. α-actin staining demonstrated the presence of medial VSMCs near the endothelial layer. Many macrophages (detected by F4/80 antibody staining) were present in aneurysmal arteries but few, if any, could be detected in control arteries (Supplemental Fig. 1).

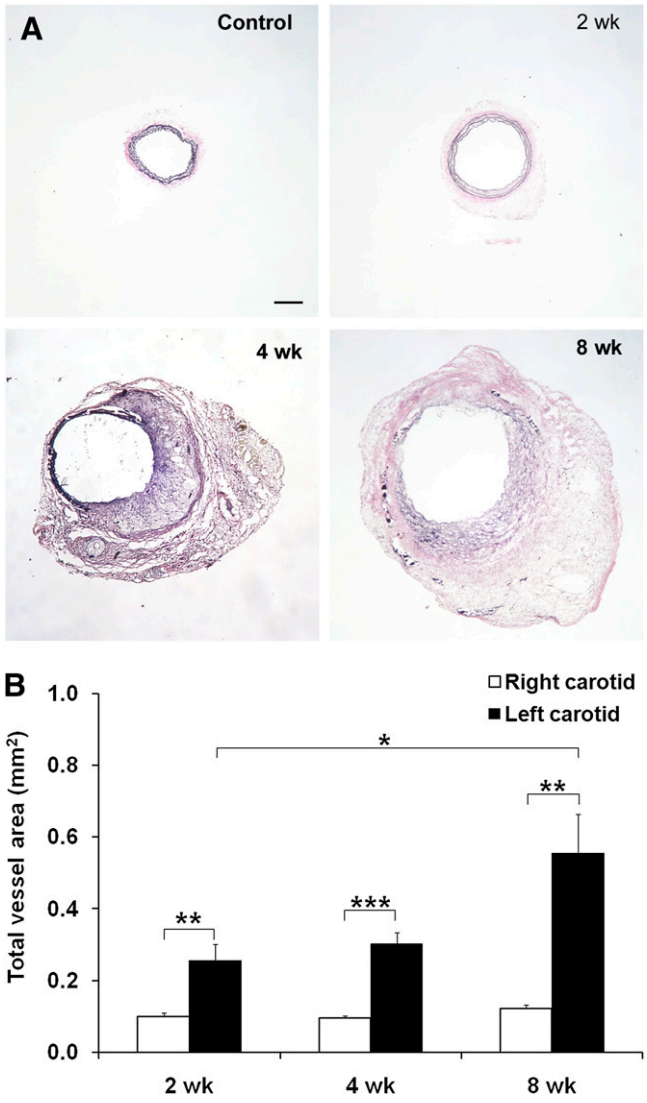

FIGURE 1. Carotid aneurysm in apoE$^{-/-}$ mice. (A) Representative examples of elastic van Gieson staining of common carotid artery exposed to NaCl (control) or at 2, 4, and 8 wk after exposure to $CaCl_2$, demonstrating marked enlargement of artery. (B) Morphometric analysis of total vessel area after exposure of left carotid artery to $CaCl_2$. n = 9–13 in each group. *$P < 0.05$. **$P = 0.01$. ***$P < 0.001$. Scale bar = 100 μm.

MMP Expression and Activation in Carotid Aneurysm

MMPs play a key role in the development of aneurysms. Therefore, we assessed the expression of several vascular

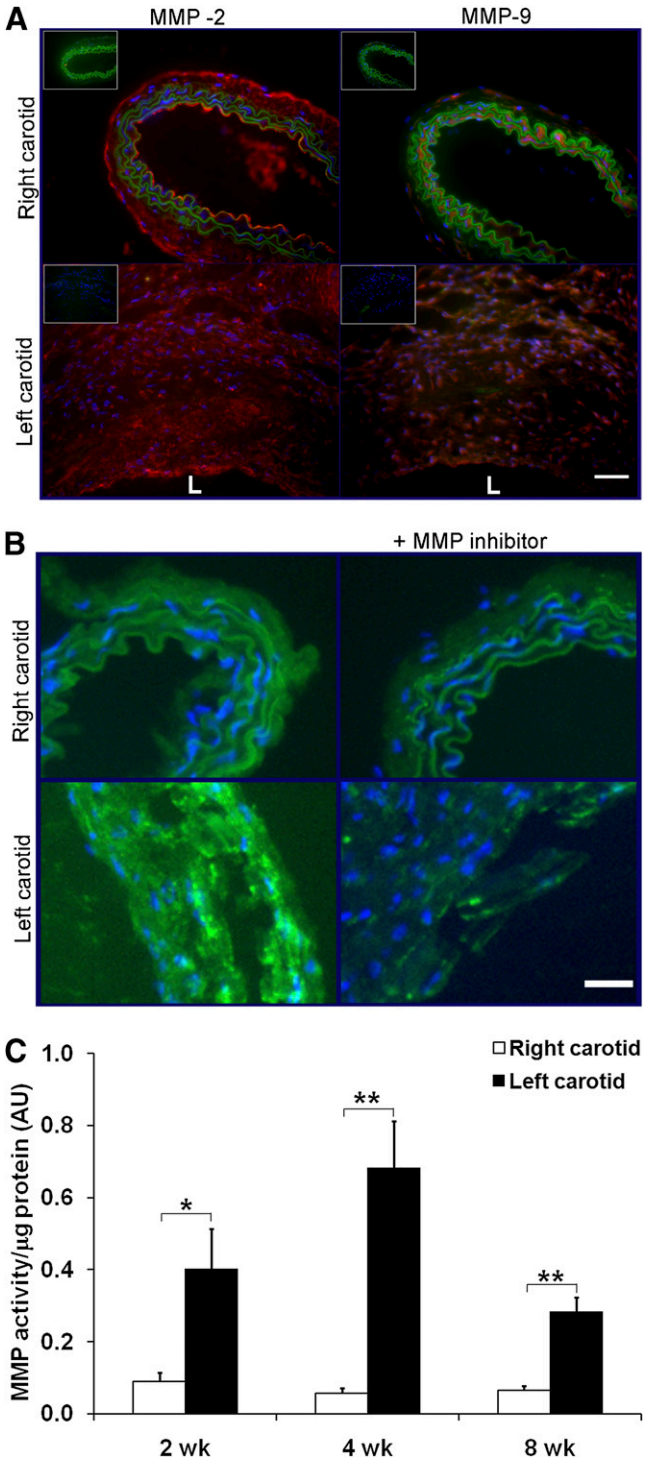

FIGURE 2. MMP expression and activity in aneurysm. (A) Representative examples of MMP-2 and MMP-9 immunofluorescent staining (in red) of carotid arteries at 4 wk, demonstrating diffuse MMP expression in aneurysmal left carotid artery. Elastic membranes are detected by their autofluorescence in green. Nuclei are detected by DAPI in blue. Insets represent staining with control antibodies. Scale bar = 100 μm. (B) Examples of in situ gelatinase zymography of control (right) and aneurysmal (left) carotid arteries at 4 wk. Protease activity is markedly reduced in presence of specific MMP inhibitors (1,10-phenanthroline). Nuclei are detected by DAPI in blue. Scale bar = 20 μm. (C) MMP activity quantified using generic fluorogenic assay at 2, 4, and 8 wk after $CaCl_2$ application. n = 9–13. $^*P < 0.05$. $^{**}P < 0.01$. AU = arbitrary units; L = lumen.

MMPs, including gelatinases and elastase (*6*), in carotid aneurysm. MMP-2 and -9 were detectable in aneurysmal arteries and exhibited a diffuse staining pattern consistent with their secreted nature (Fig. 2A). A similar staining pattern was observed for 2 MMPs with elastase activity, MMP-7 and -12 (Supplemental Fig. 2). The temporal pattern of MMP expression was addressed by quantitative reverse-transcription PCR and was found to vary among different MMPs (Supplemental Fig. 3). MMP-2 expression was rapidly upregulated after $CaCl_2$ application and reached the maximal level at 2 wk, whereas MMP-9 expression peaked at 4 wk. Similarly, MMP-3 expression increased with time and reached its maximal level at 4 wk. MMP-12 and MMP-13 expression demonstrated a gradual and late induction, reaching their maximal levels at 8 wk after surgery.

In addition to expression level, MMP activation state and the level of inhibitors present regulate MMP activity. Therefore, we assessed MMP protease activity in the vessel wall by gelatinase in situ zymography at 4 wk (Fig. 2B). Gelatinase activity was present in a diffuse pattern in aneurysmal carotid arteries, whereas sham-operated arteries exhibited minimal activity. MMP specificity of this protease activity was established by its marked reduction in the presence of a specific inhibitor, 1,10-phenanthroline. As a prelude to imaging studies, MMP activity in the vessel wall at different times after surgery was quantified using a generic MMP activity assay. Compared with control carotid arteries, MMP activity in the left carotid artery was significantly higher in $CaCl_2$-treated left carotid arteries at 2 (0.40 ± 0.11 vs. 0.09 ± 0.02 arbitrary units, $n = 5$, $P < 0.05$), 4 (0.68 ± 0.13 vs. 0.06 ± 0.02 arbitrary units, $n = 8$, $P < 0.01$), and 8 wk (0.28 ± 0.04 vs. 0.07 ± 0.01 arbitrary units, $n = 4$, $P < 0.01$) after surgery (Fig. 2C).

Micro-SPECT/CT of MMP Activation in Arterial Aneurysm

RP782, an ^{111}In-labeled tracer targeting the MMP activation epitope (*11*), was used to detect and quantify MMP activation by scintigraphic imaging in apoE$^{-/-}$ mice at 2, 4, or 8 wk after surgery. Micro-SPECT was followed by CT angiography to localize carotid arteries. On micro-SPECT/CT images, RP782 signal was clearly detectable in aneurysmal, but not control, carotid arteries (Fig. 3A; Supplemental Video 1). Imaging-derived quantitative analysis of tracer uptake demonstrated a significant difference in target-to-background activity between the aneurysmal (left) and control (right) carotid arteries (2.44 ± 0.09 and 1.29 ± 0.02, respectively, for left and right carotid arteries, $n = 51$, $P < 0.001$). Background-corrected tracer uptake in the left carotid artery peaked at 4 wk after surgery and was

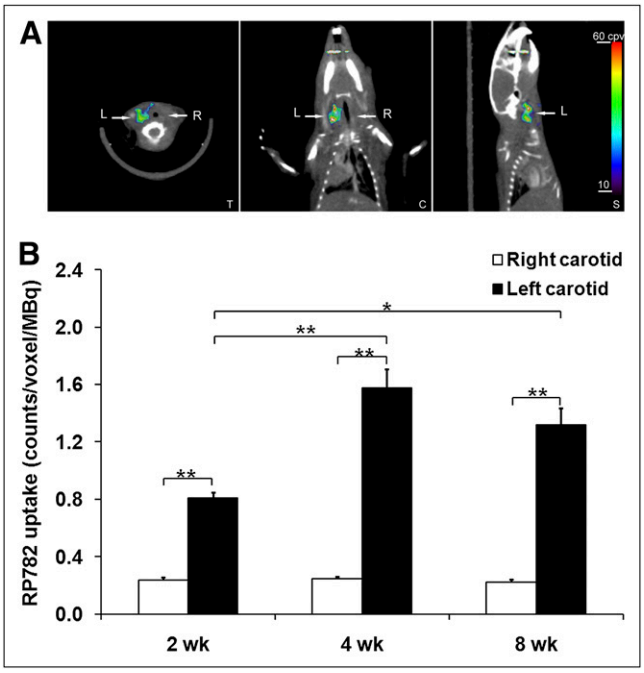

FIGURE 3. In vivo imaging of MMP activation in aneurysm. (A) Example of fused micro-SPECT/CT images of mouse at 4 wk after surgery to induce carotid aneurysm. Arrows point to aneurysmal left (L) and control right (R) carotid arteries. (B) Image-derived quantitative analysis of background-corrected RP782 carotid uptake. Background-corrected tracer uptake in left carotid artery peaked at 4 wk after surgery and was significantly higher than uptake in right carotid artery at every time point studied. n = 16–18 in each group. *P = 0.01. **$P < 0.001$. C = coronal slice; S = sagittal slice; T = transverse slice.

significantly higher than the uptake in the right carotid artery at each time point studied (2 wk: 0.81 ± 0.04 vs. 0.23 ± 0.02 cpv/MBq, n = 16, $P < 0.001$; 4 wk: 1.58 ± 0.14 vs. 0.24 ± 0.02 cpv/MBq, n = 18, $P < 0.001$; and 8 wk: 1.32 ± 0.12 vs. 0.22 ± 0.02 cpv/MBq, n = 17, $P < 0.001$) (Fig. 3B). In some of the animals, the RP782 signal was also visible at the surgical site.

Increased RP782 uptake in aneurysmal arteries was confirmed by ex vivo autoradiography, which consistently showed higher activity in the aneurysmal left carotid artery than in the control, right carotid artery (Fig. 4A). Tracer uptake in the carotid arteries was further quantified by γ-well counting in a subgroup of animals. Consistent with in vivo imaging results, left carotid artery uptake peaked at 4 wk and was significantly higher than uptake in control, right carotid arteries (2 wk: 870 ± 160 vs. 88 ± 11 cpm/MBq, n = 8, $P < 0.001$; 4 wk: 1,251 ± 367 vs. 103 ± 33 cpm/MBq, n = 9, $P < 0.001$; and 8 wk: 445 ± 56 vs. 84 ± 15 cpm/MBq, n = 9, $P < 0.001$, Fig. 4B). There was an excellent correlation between in vivo and ex vivo quantification of carotid uptake (Pearson r = 0.77, P = 0.001), establishing the validity of in vivo measurements for the following longitudinal studies. Furthermore, RP782 uptake

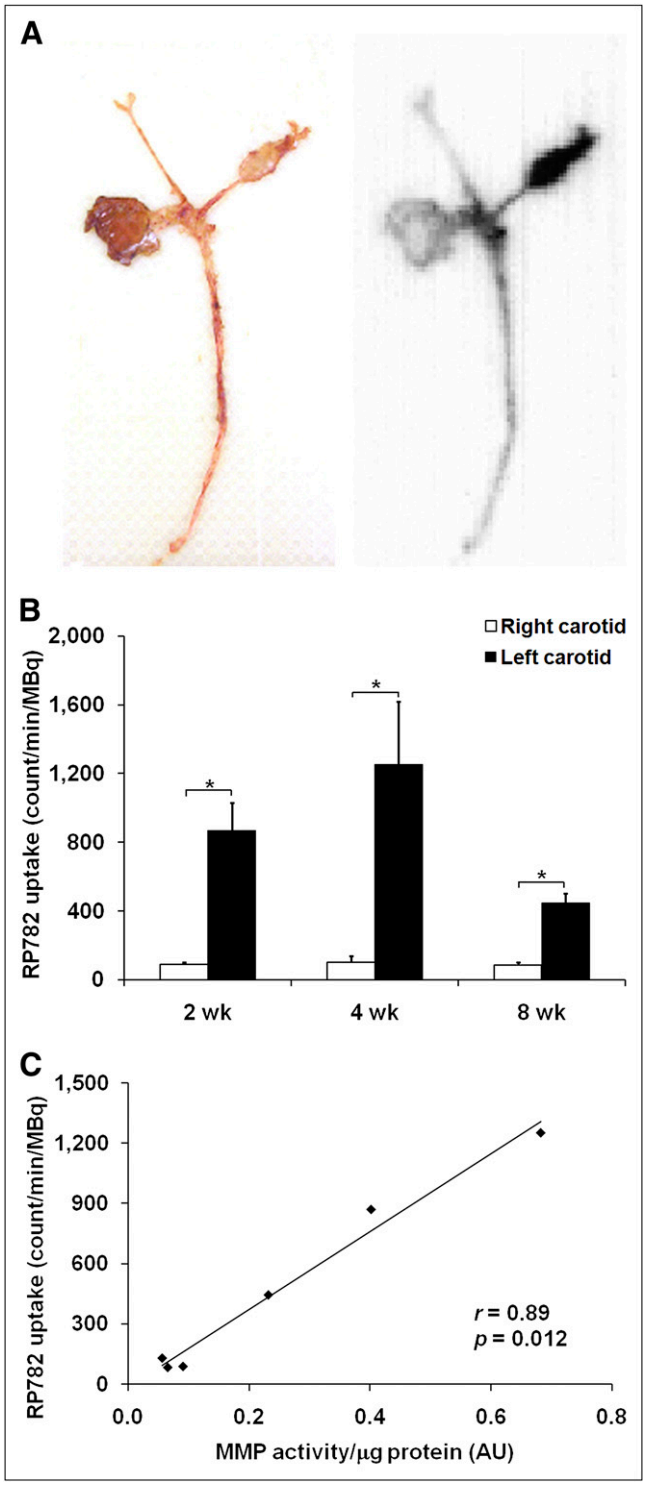

FIGURE 4. Ex vivo analysis of MMP tracer uptake in aneurysm. (A) Example of carotid arteries and aorta at 4 wk after aneurysm induction, harvested and photographed after RP782 imaging (left), with corresponding autoradiography (right). Figure represents data from at least 5 animals from each time point. (B) Quantitative analysis of RP782 uptake by γ-well counting. n = 8–9 in each group. *$P < 0.001$. (C) Correlation between carotid RP782 uptake and MMP activity assessed by quantitative zymography. AU = arbitrary units.

significantly correlated with MMP activity assessed by quantitative zymography (Spearman $r = 0.89$, $P = 0.01$, Fig. 4C).

Specificity

The specificity of RP782 uptake in aneurysmal arteries was addressed in a group of animals at 4 wk after surgery. Administration of a 50-fold excess of nonlabeled precursor significantly reduced left carotid RP782 uptake detected by micro-SPECT/CT in vivo (from 1.58 ± 0.13 cpv/MBq [$n = 18$] to 0.09 ± 0.07 cpv/MBq [$n = 2$], $P < 0.01$) (Figs. 5A and 5B; Supplemental Video 2). The blocking effect of nonlabeled precursor on tracer uptake in the aneurysm (and nonaneursmal arteries) was clearly visible on carotid autoradiography (Supplemental Fig. 4). A broad-spectrum MMP inhibitor, 1,10-phenanthroline, significantly inhibited ex vivo RP782 binding to carotid aneurysms (from 3.2 ± 0.6 cpm/kBq to 0.4 ± 0.2 cpm/kBq, $n = 6$, $P < 0.05$) (Supplemental Fig. 5), further confirming the MMP specificity of RP782 uptake in this model.

MMP Activation and Aneurysm Expansion

Given the causal role of MMP activation in the pathogenesis of aneurysm, we sought to establish whether quantitation of MMP activation by scintigraphic imaging can provide information on subsequent aneurysm size in individual animals. In a longitudinal study, we sequentially imaged a group of animals at 2 and 4 wk after surgery, after which the carotid arteries were harvested for morphometric analysis. We found no significant correlation between tracer uptake and aneurysm size at 4 wk (data not shown). However, MMP tracer uptake at 2 wk significantly correlated with the aneurysm size at 4 wk (Pearson $r = 0.69$, $n = 11$, $P = 0.02$) (Fig. 6).

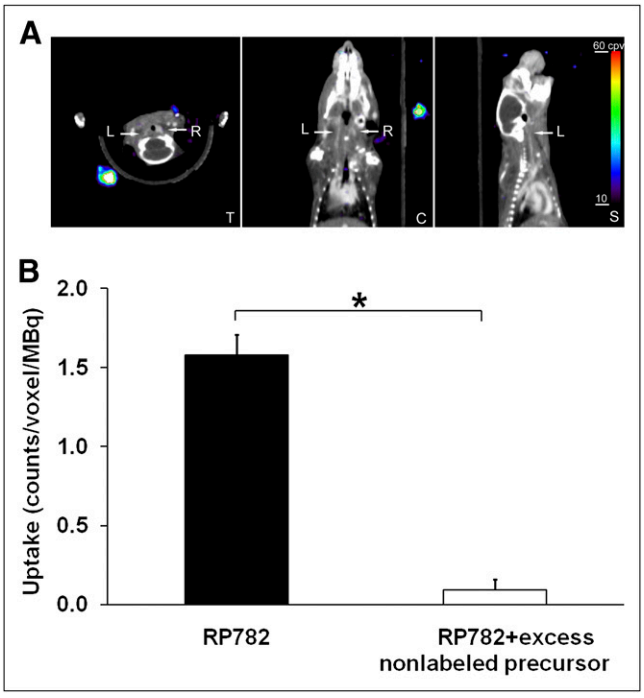

FIGURE 5. MMP tracer uptake specificity. (A) Example of RP782 micro-SPECT/CT after administration of 50-fold excess of precursor in mouse 4 wk after surgery to induce carotid aneurysm. Arrows point to aneurysmal left (L) and control right (R) carotid arteries. (B) Image-derived quantitative analysis of RP782 carotid uptake in absence ($n = 18$) or presence ($n = 2$) of 50-fold excess of nonlabeled precursor. *$P < 0.01$. C = coronal slice; S = sagittal slice; T = transverse slice.

DISCUSSION

Arterial aneurysm affects various vascular beds and is an important cause of morbidity and mortality in most countries, including the United States, where abdominal aortic aneurysm (AAA) alone is responsible for approximately 15,000–30,000 deaths every year (*16,17*). The high prevalence of aneurysm and the morbidity of its complications have led to the institution of national screening programs in high-risk populations (e.g., middle-aged men with a smoking history) (*3,18*). Existing aneurysm imaging modalities (ultrasonography, CT, and MRI) provide little information beyond the artery size. Although size is a good predictor of the risk of rupture and dissection of an aneurysm, many complications occur in smaller aneurysms that do not meet the clinical and imaging criteria for surgical repair (*4,5,19*). Rapid expansion of aneurysm increases the risk of rupture and dissection. However, at the present time, aneurysm expansion can be detected only retrospectively through serial imaging. Molecular imaging targeted at relevant molecular and cellular features of aneurysm can potentially address the limitations of existing imaging modalities, help identify patients at high risk for complications, and provide novel opportunities to study aneurysm biology in longitudinal studies.

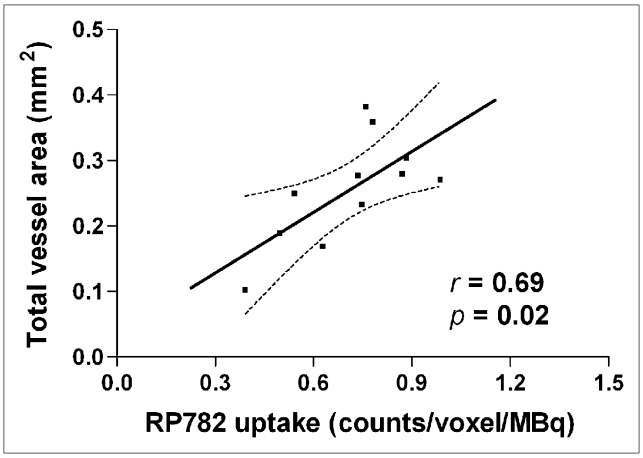

FIGURE 6. MMP activation and aneurysm size. There is significant correlation between MMP tracer uptake in aneurysmal carotid artery at 2 wk and total vessel area measured at 4 wk in same animal. $n = 11$. Dotted lines represent 95% confidence interval.

In an aneurysm, the imbalance between matrix synthesis and degradation and cell proliferation and death creates an arterial wall with reduced tensile strength, which is prone to expansion, rupture, or dissection under the influence of hemodynamic forces. Vessel wall inflammation plays a key role in this process (*20*). Inflammatory and other vascular cells produce high levels of activated proteases, including MMPs, which through digestion of collagen and elastin participate in the weakening of the vessel wall and facilitate recruitment of additional inflammatory cells (*21*). Cytokines, reactive oxygen species, prostaglandin derivatives, and other mediators released by inflammatory cells induce VSMC death and media hypotrophy and adversely affect the ability of VSMCs to repair the matrix scaffold (*22*). As such, complicated aneurysms commonly contain a high density of inflammatory cells in conjunction with high levels of activated proteases, including MMPs (*7,17,21*). A similar pattern is observed in various experimental animal models of aneurysm, all of which replicate within a few weeks a process that normally takes years to develop in humans. The $CaCl_2$ model mimics many features of human disease and has been extensively used to study the molecular mechanisms of aneurysm formation (*23–25*).

On the basis of this view of pathogenesis, imaging MMP activation in the vessel wall appears to be a promising approach to identifying aneurysms that are prone to expansion. MMPs are a multigene family of at least 23 secreted or transmembrane zinc- and calcium-dependent endopeptidases that selectively digest individual components of extracellular matrix and other proteins and play a key role in vascular remodeling (*6,10*). The causal role of MMPs in the expansion of aneurysm is supported by several lines of evidence. Histologic studies demonstrate differences in MMP expression and activity between normal arteries and aneurysms of different sizes or those ruptured (*7,26,27*). Targeted disruption of specific members of the MMP family reduces aneurysm formation in animal models (*8,9,28,29*). MMP inhibitors (e.g., doxycycline) inhibit aneurysm formation in animal models, a finding that has raised the possibility of treating MMP expansion in humans using similar agents (*8*). Expression, activation, and inhibition by tissue inhibitors of matrix metalloproteinases (TIMPs) are the main regulatory mechanisms of MMP activity. MMPs are biosynthesized either as secreted or transmembrane proenzymes. Activation of these latent MMPs is achieved through enzymatic cleavage of the propeptide, which exposes a common catalytic domain (*10*). Several broad-spectrum MMP inhibitors bind to and inactivate this domain. Tracers used in this study are structurally based on broad-spectrum MMP inhibitors and bind with high specificity to the exposed catalytic domain (*11,13*). This process enabled us to simultaneously detect activation of several MMPs by molecular imaging in vivo. Because MMP activation is a common pathophysiologic feature of aneurysm in different arterial beds, we focused on imaging carotid arteries to circumvent technical challenges associated with imaging the aorta in the mouse, in which the proximity of the aorta to the urinary bladder and kidneys complicates signal detection and quantification. We demonstrated that MMP activation can be imaged as early as 2 wk and peaks at 4 wk in this murine model of aneurysm. Tracer uptake in the surgical wound was a confounding factor, which was dealt with by localizing the target arteries by CT angiography. Ex vivo assessment of tracer uptake by γ-well counting further confirmed that the tracer localizes in the aneurysm. The target-to-background ratio in the aneurysm was sufficient for micro-SPECT of carotid aneurysm in the mouse. It remains to be empirically determined whether high enough ratios for imaging can be obtained with human aneurysm.

The data on MMP plasma levels and aneurysm growth are inconclusive (*30*). This uncertainty may be explained by the fact that in addition to MMP expression in the aneurysm, MMP plasma levels may be influenced by other factors. In normal arteries MMP-2, TIMP-1, and TIMP-2 are produced constitutively by endothelial cells and VSMCs, but no in situ enzymatic activity is detectable (*6*). Here, we demonstrated that in addition to MMP-2 and MMP-9, which play an important role in the development of aneurysm (*9*), other MMPs (including MMP-3, -12, and -13) are also upregulated in aneurysm. Major differences were detected in the time course of MMP expression, suggesting that each MMP plays a distinct role in the pathogenesis. There is no established method for detecting focal activation of specific MMPs in vivo. Using a tracer with specificity for the MMP activation epitope, we were able to simultaneously detect activation of multiple MMPs and demonstrated that this approach can be used to predict the subsequent aneurysm size. Tracers targeted at individual members of the MMP family are in development (*31–33*). Given major differences in the expression pattern of different MMPs and lack of experimental data on their activation, it remains to be empirically determined if in vivo imaging of any specific member of the MMP family will provide more robust information on the propensity of an aneurysm to expansion.

A nonspecific marker of inflammation, ^{18}F-FDG has been assessed for the detection of inflammation and propensity to complications in human studies (*34–36*) and found to be insufficiently sensitive and specific (*37*). MMP imaging, used previously by our group (*12*) and others (*13,38,39*) to image MMP activation in injury-induced vascular remodeling and atherosclerosis, targets a process directly linked to extracellular matrix remodeling. With its potentially better specificity for remodeling, it appears to be a promising alternative approach to imaging aneurysm biology. However, it remains to be empirically determined whether this approach has a better specificity and sensitivity than ^{18}F-FDG. The quantitative nature of scintigraphic imaging allowed us to accurately quantify tracer uptake in carotid arteries. Not unexpectedly, there was no significant correlation between RP782 uptake and expression of each

specific member of the MMP family (data not shown). In the absence of a better alternative, we relied on a generic MMP substrate to assess MMP activation and correlate it with RP782 uptake. Despite differences in relative affinity of individual MMPs for RP782 and this substrate, we detected a strong correlation between these 2 independent measures of MMP activation. Finally, whereas MMP activation detected by scintigraphic imaging and aneurysm size at 4 wk did not correlate, tracer uptake at 2 wk correlated well with the aneurysm size at 4 wk, establishing MMP-targeted molecular imaging as a tool for predicting future expansion of an aneurysm.

CONCLUSION

MMP-targeted imaging provides a tool for studying aneurysm biology, its prognosis, and its response to therapy. It remains to be empirically determined if other molecular and cellular targets (e.g., specific MMPs or other proteases) can serve as alternative or complementary approaches to MMP-targeted imaging of aneurysm biology. Ultimately, prospective identification of aneurysms that are prone to expansion will help identify and treat these high-risk aneurysms and potentially reduce aneurysm morbidity and mortality.

ACKNOWLEDGMENTS

This work was supported by National Institutes of Health R01 HL85093, Program Project HL70295, a Department of Veterans Affairs Merit Award, and a research award from the American Society of Nuclear Cardiology. D. Scott Edwards and Michael Azure are employees of Lantheus Medical Imaging. Albert Sinusas and Mehran Sadeghi receive experimental tracers from Lantheus Medical Imaging. In addition, Albert Sinusas has received research grants from Lantheus Medical Imaging.

REFERENCES

1. Davies MJ. Aortic aneurysm formation: lessons from human studies and experimental models. *Circulation.* 1998;98:193–195.
2. El-Hamamsy I, Yacoub MH. Cellular and molecular mechanisms of thoracic aortic aneurysms. *Nat Rev Cardiol.* 2009;6:771–786.
3. Cosford PA, Leng GC. Screening for abdominal aortic aneurysm. *Cochrane Database Syst Rev.* April 2007:CD002945.
4. Ashton HA, Buxton MJ, Day NE, et al. The Multicentre Aneurysm Screening Study (MASS) into the effect of abdominal aortic aneurysm screening on mortality in men: a randomised controlled trial. *Lancet.* 2002;360:1531–1539.
5. Lederle FA, Wilson SE, Johnson GR, et al. Immediate repair compared with surveillance of small abdominal aortic aneurysms. *N Engl J Med.* 2002;346:1437–1444.
6. Galis ZS, Khatri JJ. Matrix metalloproteinases in vascular remodeling and atherogenesis: the good, the bad, and the ugly. *Circ Res.* 2002;90:251–262.
7. Thompson RW, Holmes DR, Mertens RA, et al. Production and localization of 92-kilodalton gelatinase in abdominal aortic aneurysms: an elastolytic metalloproteinase expressed by aneurysm-infiltrating macrophages. *J Clin Invest.* 1995;96:318–326.
8. Pyo R, Lee JK, Shipley JM, et al. Targeted gene disruption of matrix metalloproteinase-9 (gelatinase B) suppresses development of experimental abdominal aortic aneurysms. *J Clin Invest.* 2000;105:1641–1649.
9. Longo GM, Xiong W, Greiner TC, Zhao Y, Fiotti N, Baxter BT. Matrix metalloproteinases 2 and 9 work in concert to produce aortic aneurysms. *J Clin Invest.* 2002;110:625–632.
10. Visse R, Nagase H. Matrix metalloproteinases and tissue inhibitors of metalloproteinases: structure, function, and biochemistry. *Circ Res.* 2003;92:827–839.
11. Su H, Spinale FG, Dobrucki LW, et al. Noninvasive targeted imaging of matrix metalloproteinase activation in a murine model of postinfarction remodeling. *Circulation.* 2005;112:3157–3167.
12. Zhang J, Nie L, Razavian M, et al. Molecular imaging of activated matrix metalloproteinases in vascular remodeling. *Circulation.* 2008;118:1953–1960.
13. Fujimoto S, Hartung D, Ohshima S, et al. Molecular imaging of matrix metalloproteinase in atherosclerotic lesions: resolution with dietary modification and statin therapy. *J Am Coll Cardiol.* 2008;52:1847–1857.
14. Chiou AC, Chiu B, Pearce WH. Murine aortic aneurysm produced by periarterial application of calcium chloride. *J Surg Res.* 2001;99:371–376.
15. Sadeghi MM, Krassilnikova S, Zhang J, et al. Detection of injury-induced vascular remodeling by targeting activated $\alpha_v\beta_3$ integrin in vivo. *Circulation.* 2004;110:84–90.
16. Kent KC, Zwolak RM, Jaff MR, et al. Screening for abdominal aortic aneurysm: a consensus statement. *J Vasc Surg.* 2004;39:267–269.
17. Ince H, Nienaber CA. Etiology, pathogenesis and management of thoracic aortic aneurysm. *Nat Clin Pract Cardiovasc Med.* 2007;4:418–427.
18. Lederle FA. Screening for AAA in the USA. *Scand J Surg.* 2008;97:139–141.
19. Lederle FA, Johnson GR, Wilson SE, et al. The aneurysm detection and management study screening program: validation cohort and final results. Aneurysm Detection and Management Veterans Affairs Cooperative Study Investigators. *Arch Intern Med.* 2000;160:1425–1430.
20. Curci JA, Thompson RW. Adaptive cellular immunity in aortic aneurysms: cause, consequence, or context? *J Clin Invest.* 2004;114:168–171.
21. Freestone T, Turner RJ, Coady A, Higman DJ, Greenhalgh RM, Powell JT. Inflammation and matrix metalloproteinases in the enlarging abdominal aortic aneurysm. *Arterioscler Thromb Vasc Biol.* 1995;15:1145–1151.
22. Walton LJ, Franklin IJ, Bayston T, et al. Inhibition of prostaglandin E2 synthesis in abdominal aortic aneurysms: implications for smooth muscle cell viability, inflammatory processes, and the expansion of abdominal aortic aneurysms. *Circulation.* 1999;100:48–54.
23. Xiong W, Knispel R, MacTaggart J, Greiner TC, Weiss SJ, Baxter BT. Membrane-type 1 matrix metalloproteinase regulates macrophage-dependent elastolytic activity and aneurysm formation in vivo. *J Biol Chem.* 2009;284:1765–1771.
24. Yoshimura K, Aoki H, Ikeda Y, Furutani A, Hamano K, Matsuzaki M. Regression of abdominal aortic aneurysm by inhibition of c-Jun N-terminal kinase in mice. *Ann N Y Acad Sci.* 2006;1085:74–81.
25. Xiong W, MacTaggart J, Knispel R, Worth J, Persidsky Y, Baxter BT. Blocking TNF-α attenuates aneurysm formation in a murine model. *J Immunol.* 2009;183:2741–2746.
26. Taketani T, Imai Y, Morota T, et al. Altered patterns of gene expression specific to thoracic aortic aneurysms: microarray analysis of surgically resected specimens. *Int Heart J.* 2005;46:265–277.
27. Wilson WR, Anderton M, Schwalbe EC, et al. Matrix metalloproteinase-8 and -9 are increased at the site of abdominal aortic aneurysm rupture. *Circulation.* 2006;113:438–445.
28. Longo GM, Buda SJ, Fiotta N, et al. MMP-12 has a role in abdominal aortic aneurysms in mice. *Surgery.* 2005;137:457–462.
29. Ikonomidis JS, Barbour JR, Amani Z, et al. Effects of deletion of the matrix metalloproteinase 9 gene on development of murine thoracic aortic aneurysms. *Circulation.* 2005;112(9, suppl):I242–I248.
30. Golledge J, Tsao PS, Dalman RL, Norman PE. Circulating markers of abdominal aortic aneurysm presence and progression. *Circulation.* 2008;118:2382–2392.
31. Lebel R, Jastrzebska B, Therriault H, et al. Novel solubility-switchable MRI agent allows the noninvasive detection of matrix metalloproteinase-2 activity in vivo in a mouse model. *Magn Reson Med.* 2008;60:1056–1065.
32. Scherer RL, VanSaun MN, McIntyre JO, Matrisian LM. Optical imaging of matrix metalloproteinase-7 activity in vivo using a proteolytic nanobeacon. *Mol Imaging.* 2008;7:118–131.
33. Watkins GA, Jones EF, Scott Shell M, et al. Development of an optimized activatable MMP-14 targeted SPECT imaging probe. *Bioorg Med Chem.* 2009;17:653–659.
34. Sakalihasan N, Van Damme H, Gomez P, et al. Positron emission tomography (PET) evaluation of abdominal aortic aneurysm (AAA). *Eur J Vasc Endovasc Surg.* 2002;23:431–436.

35. Kotze CW, Menezes LJ, Endozo R, Groves AM, Ell PJ, Yusuf SW. Increased metabolic activity in abdominal aortic aneurysm detected by ^{18}F-fluorodeoxyglucose (^{18}F-FDG) positron emission tomography/computed tomography (PET/CT). *Eur J Vasc Endovasc Surg.* 2009;38:93–99.
36. Reeps C, Essler M, Pelisek J, Seidl S, Eckstein HH, Krause BJ. Increased ^{18}F-fluorodeoxyglucose uptake in abdominal aortic aneurysms in positron emission/computed tomography is associated with inflammation, aortic wall instability, and acute symptoms. *J Vasc Surg.* 2008;48:417–423, discussion 424.
37. Kuehl H, Eggebrecht H, Boes T, et al. Detection of inflammation in patients with acute aortic syndrome: comparison of FDG-PET/CT imaging and serological markers of inflammation. *Heart.* 2008;94:1472–1477.
38. Schafers M, Riemann B, Kopka K, et al. Scintigraphic imaging of matrix metalloproteinase activity in the arterial wall in vivo. *Circulation.* 2004;109:2554–2559.
39. Ohshima S, Petrov A, Fujimoto S, et al. Molecular imaging of matrix metalloproteinase expression in atherosclerotic plaques of mice deficient in apolipoprotein e or low-density-lipoprotein receptor. *J Nucl Med.* 2009;50:612–617.